

# Theoretical interpretation of the experimental electronic structure of lens shaped, self-assembled InAs/GaAs quantum dots

A. J. Williamson, L.W. Wang, and Alex Zunger

*National Renewable Energy Laboratory, Golden, CO 80401*

We adopt an atomistic pseudopotential description of the electronic structure of self-assembled, lens shaped InAs quantum dots within the “linear combination of bulk bands” method. We present a detailed comparison with experiment, including quantities such as the single particle electron and hole energy level spacings, the excitonic band gap, the electron-electron, hole-hole and electron hole Coulomb energies and the optical polarization anisotropy. We find a generally good agreement, which is improved even further for a dot composition where some Ga has diffused into the dots.

## I. INTRODUCTION: USING THEORY AS A BRIDGE BETWEEN THE STRUCTURE AND THE ELECTRONIC PROPERTIES OF QUANTUM DOTS

Self-assembled, Stranski-Krastanow (SK) grown semiconductor quantum dots have recently received considerable attention as they exhibit a rich spectrum of phenomena including quantum-confinement[1, 2, 3], exchange-splittings[4], Coulomb charging/blockade[5, 6, 7, 8, 9, 10, 11, 12, 13] and multi-exciton transitions[4, 14]. Over the past few years a considerable number of high quality measurements of the electronic level structure of these dot systems have been performed, using photoluminescence (PL)[10, 12, 15, 16, 17, 18, 19, 20], photoluminescence luminescence excitation (PLE)[4, 14], capacitance[5, 6, 7, 13] and far infra red (FIR) spectroscopy[7, 21, 22, 23, 24]. These measurements have been able to determine the electronic level structure to relatively high precision. In parallel with these measurements, several groups have also attempted to measure the geometry and composition of these dots[15, 16, 25, 26, 27]. So far, however, these measurements have failed to provide details of the shape, size, inhomogeneous strain and alloying profiles to a similar level of accuracy to that in which the electronic structure has been determined. As a result, the size of the dots were often used as adjustable parameters in models that fit experimental spectra. For example, using a single-band effective mass model, Dekel *et. al*[14] defined an “effective shape” (cuboid) and “effective dimension” that reproduced the measured excitonic transitions. Similar “parabolic dot” models have been assumed by Hawrylak *et. al*[1].

The accuracy of single-band and multi-band effective mass methods was recently examined in a series of papers [28, 29, 30, 31, 32]. In these works, the shape, size and composition of nanostructures were arbitrarily fixed, and the electronic structure was evaluated by successively improving the basis set, starting from single-band methods (effective-mass), going to six and eight band methods (k.p), and finally, using a converged, multi-

band approach (plane-wave pseudopotentials). It was found that conventional effective-mass and k.p methods can sometimes significantly misrepresent the fully converged results even when the shape, size and composition was given. The observed discrepancies were both quantitative (such as band gap values, level spacings, Coulomb energies) and qualitative (absence of polarization anisotropy in square based pyramidal dots[32], missing energy levels[30]). As a result of these limitations these methods may not offer a reliable bridge between the electronic structure and atomic structure.

In this paper, we offer a bridge between recent measurements of the *electronic structure* and measurements of the *atomic structure* of the dots using accurate theoretical modeling. Modeling can determine if the calculated electronic structure resulting from an assumed shape, size, strain and alloying profiles agrees with the measured electronic structure or not. A theory that can perform such a “bridging function” must be accurate and reliable. The pseudopotential approach to this problem qualifies, in that any discrepancy between the predicted and measured electronic properties can be attributed to incorrectly assumed shape, size or alloying profile. We have studied a range of shapes, sizes and alloy profiles and find that a lens-shaped InAs dot with an inhomogeneous Ga alloying profile is in closest agreement with current measurements. In the following sections we attempt to provide a consistent theoretical interpretation of numerous spectroscopic properties of InAs/GaAs dots.

## II. OUTLINE OF THE METHOD OF CALCULATION

We aim to calculate the energy associated with various electronic excitations in InAs/GaAs quantum dots. These energies can be expressed as total energy differences and require four stages of calculation:

(i) *Assume the shape, size and composition and compute the equilibrium displacements:* We first construct a supercell containing both the quantum dot and sur-

rounding GaAs barrier material. The shape, size and composition profile are taken as input and subsequently refined. Sufficient GaAs barrier is used, so that when periodic boundary conditions are applied to the system, the electronic and strain interactions between dots in neighboring cells is negligible. The atomic positions within the supercell are then relaxed by minimizing the strain energy described by an atomistic force field[33, 34] including bond bending, bond stretching and bond bending-bond stretching interactions (see section III A). An atomic force field is similar to continuum elasticity approaches[34] in that both methods are based on the elastic constants,  $\{C_{ij}\}$ , of the underlying bulk materials. However, atomistic approaches are superior to continuum methods in two ways, (a) they can contain anharmonic effects, and (b) they capture the correct point group symmetry, e.g. the point group symmetry of a square based, zinc blende pyramidal dot is  $C_{2v}$ , since the [110] and [110] directions are inequivalent while continuum methods[34], find  $C_{4v}$ . More details of the atomistic relaxation are given in section III A.

(ii) *Setup and solve the pseudopotential single-particle equation:* A single-particle Schrödinger equation is set up at the relaxed atomic positions,  $\{\mathbf{R}_{n\alpha}\}$

$$\hat{H}\psi_i(\mathbf{r}) = \left\{ -\frac{\beta}{2}\nabla^2 + \sum_{n\alpha} \hat{v}_\alpha(\mathbf{r} - \mathbf{R}_{n\alpha}) \right\} \psi_i(\mathbf{r}) = \epsilon_i \psi_i(\mathbf{r}) . \quad (1)$$

The potential for the system is written as a sum of strain-dependent, screened atomic pseudopotentials,  $v_\alpha$ , that are fit to bulk properties extracted from experiment and first-principles calculations (see section III B). The Schrödinger equation is solved by expanding  $\psi$  in a linear combination of bulk states,  $\phi_{nk}$ , from bands,  $n$ , and k-points,  $k$ ,

$$\psi_i(\mathbf{r}, \epsilon) = \sum_{n,k} c_{n,k}^{(i)} \phi_{nk}(\mathbf{r}, \epsilon) , \quad (2)$$

taken at a few strain values. The solution of Eqs. (1) and (2) provides the level structure and dipole transition matrix elements. More details on the solution of the Schrödinger equation are given in section III C.

(iii) *Calculate the screened, inter-particle many-body interactions:* The calculated single particle wavefunctions are used to compute the electron-electron, electron-hole and hole-hole direct,  $J_{ee}, J_{eh}, J_{hh}$ , and exchange  $K_{ee}, K_{eh}, K_{hh}$  Coulomb energies (see section III D).

(iv) *Calculate excitation energies as differences in total, many particle energies:* For example, the difference between the total energy  $E_{11}[h_0^1 e_0^1]$  of a dot with a hole in level  $h_0$  and an electron in level  $e_0$  and the total energy  $E_{00}[h_0^0 e_0^0]$  of the unexcited dot is

$$E_{11}[h_0^1 e_0^1] - E_{00}[h_0^0 e_0^0] = (\epsilon_{e_0} - \epsilon_{h_0}) - J_{e_0 h_0} + 2K_{e_0 h_0} \delta_{S,0} , \quad (3)$$

where (in the absence of spin-orbit coupling)  $\delta_{S,0} = 1$  for triplet states, and 0 for singlet states. Analogous

expressions exist for electron-addition experiments (see section III D).

The main approximations involved in our method are: (a) the fit of the pseudopotential to the experimental data of bulk materials is never perfect (see Table I) and (b) we neglect self-consistent iterations in that we assume that the screened pseudopotential drawn from a bulk calculation is appropriate for the dot. Our numerical convergence parameters are (i) the size of the GaAs barrier separating periodic images of the dots, and (ii) the number of bulk wavefunctions used in the LCBB expansion of the wavefunctions. To examine the effects of these approximations and convergences on the ultimate level of accuracy that can be obtained with our methodology we have first applied these methods to an InGaAs/GaAs quantum well (see section III E), where experimental measurements of the shape, size, composition and transition energies are more established (see section III E). We next describe the details of our method.

TABLE I: Fitted bulk electronic properties for GaAs and InAs using the screened atomic pseudopotentials, in Eq.(7). The hydrostatic deformation potential of the band gap and  $\Gamma_{15v}$  levels are denoted by  $a_{gap}$  and  $a_{\Gamma_{15v}}$ . The biaxial deformation potential is denoted by  $b$  and the spin-orbit splittings at the  $\Gamma_{15v}$  and  $L_{1v}$  points are denoted by  $\Delta_0$  and  $\Delta_1$ .

Property	GaAs		InAs	
	EPM	Expt[39]	EPM	Expt[39]
$E_{gap}$	1.527	1.52	0.424	0.42
$E_{X_{5v}}$	-2.697	-2.96	-2.330	-2.40
$E_{X_{1c}}$	1.981	1.98	2.205	2.34
$E_{X_{3c}}$	2.52	2.50	2.719	2.54
$E_{L_{3v}}$	-1.01	-1.30	-5.76	-6.30
$E_{L_{1c}}$	2.36	1.81	1.668	1.71
$m_e^*$	0.066	0.067	0.024	0.023
$m_{lh}^*[100]$	0.342	0.40	0.385	0.35
$m_{lh}^*[111]$	0.866	0.57	0.994	0.85
$m_{lh}^*[100]$	0.093	0.082	0.030	0.026
$a_{gap}$	-7.88	-8.33	-6.79	-5.7
$a_{\Gamma_{15v}}$	-1.11	-1.0	-0.826	-1.0
$b$	-1.559	-1.7	-1.62	-1.7
$\Delta_0$	0.34	0.34	0.36	0.38
$\Delta_1$	0.177	0.22	0.26	0.27

### III. DETAILS OF THE METHOD OF CALCULATIONS

#### A Calculation of equilibrium atomic positions for a given shape

To calculate the relaxed atomic positions within the supercell, we use a generalization (G-VFF) of the original valence force field (VFF)[33] model. Our implementation of the VFF includes bond stretching, bond angle bending and bond-length/bond-angle interaction terms

in the VFF Hamiltonian. This enables us to accurately reproduce the  $C_{11}$ ,  $C_{12}$  and  $C_{44}$  elastic constants in a zincblende bulk material. We have also included higher order bond stretching terms, which lead to the correct dependence of the Young's modulus with pressure. The G-VFF total energy can be expressed as:

$$E_{VFF} = \sum_i \sum_j^{nni} \frac{3}{8} [\alpha_{ij}^{(1)} \Delta d_{ij}^2 + \alpha_{ij}^{(2)} \Delta d_{ij}^3] + \sum_i \sum_{k>j}^{nni} \frac{3\beta_{jik}}{8d_{ij}^0 d_{ik}^0} [(\mathbf{R}_j - \mathbf{R}_i) \cdot (\mathbf{R}_k - \mathbf{R}_i) - \cos\theta_{jik}^0 d_{ij}^0 d_{ik}^0]^2 + \sum_i \sum_{k>j}^{nni} \frac{3\sigma_{ijk}}{d_{ik}^0} \Delta d_{ij} [(\mathbf{R}_j - \mathbf{R}_i) \cdot (\mathbf{R}_k - \mathbf{R}_i) - \cos\theta_{jik}^0 d_{ij}^0 d_{ik}^0], \quad (4)$$

where  $\Delta d_{ij}^2 = [(R_i - R_j)^2 - d_{ij}^{0,2}] / d_{ij}^0$ . Here  $\mathbf{R}_i$  is the coordinate of atom  $i$  and  $d_{ij}^0$  is the ideal (unrelaxed) bond distance between atom types of  $i$  and  $j$ . Also,  $\theta_{jik}^0$  is the ideal (unrelaxed) angle of the bond angle  $j - i - k$ . The  $\sum^{nni}$  denotes summation over the nearest neighbors of atom  $i$ . The bond stretching, bond angle bending, and bond-length/bond-angle interaction coefficients  $\alpha_{ij}^{(1)}$  ( $\equiv \alpha$ ),  $\beta_{jik}$ ,  $\sigma_{ijk}$  are related to the elastic constants in a pure zincblende structure in the following way,

$$\begin{aligned} C_{11} + 2C_{12} &= \frac{\sqrt{3}}{4d_0} (3\alpha + \beta - 6\sigma) \\ C_{11} - C_{12} &= \frac{\sqrt{3}}{d_0} \beta \\ C_{44} &= \frac{\sqrt{3}}{d_0} \frac{[(\alpha + \beta)(\alpha\beta - \sigma^2) - 2\sigma^3 + 2\alpha\beta\sigma]}{(\alpha + \beta + 2\sigma)^2} \end{aligned} \quad (5)$$

The second-order bond stretching coefficient  $\alpha^{(2)}$  is related to the pressure derivative of the Young's modulus by  $\frac{dB}{dP}$ , where  $B = (C_{11} + 2C_{12})/3$  is the Young's modulus. Note that in the standard[33] VFF which we have used previously[35, 36, 37] the last terms of Eq.(4) are missing, so  $\sigma = 0$  in Eq.(5). Thus there were only *two* free parameters ( $\alpha, \beta$ ) and therefore three elastic constants could not, in general, be fit exactly. The G-VFF parameters and the resulting elastic constants are shown in Table II for GaAs and InAs crystals. For an InGaAs alloy system, the bond angle and bond-length/bond-angle interaction parameters  $\beta, \sigma$  for the mixed cation Ga-As-In bond-angle are taken as the algebraic average of the In-As-In and Ga-As-Ga values. The ideal bond angle  $\theta_{jik}^0$  is  $109^\circ$  for the pure zincblende crystal. However, to satisfy Vegas's law for the alloy volume, we find that it is necessary to use  $\theta_{Ga-As-In}^0 = 110.5^\circ$  for the cation mixed bond angle.

As a simple test of this G-VFF for alloy systems, we compared the relaxed atomic positions from G-VFF with pseudopotential LDA results for a (100)

TABLE II: Input G-VFF parameters  $\alpha, \beta, \sigma$  to Eq.(4) and their resulting elastic constants  $C_{11}$ ,  $C_{12}$  and  $C_{44}$  ( $10^3$  dyne/cm).

	$\alpha$	$\beta$	$\sigma$	$\alpha^{(2)}$	$C_{11}$	$C_{12}$	$C_{44}$
GaAs	32.153	9.370	-4.099	-105.	12.11	5.48	6.04
InAs	21.674	5.760	-5.753	-112.	8.33	4.53	3.80

$(\text{GaAs})_1/(\text{InAs})_1$  superlattice where the  $c/a$  ratio is fixed to 1, but we allow energy minimizing changes in the overall lattice constant ( $a_{eq}$ ) and the atomic internal degrees of freedom ( $u_{eq}$ ). We find  $a_{eq}^{LDA} = 5.8612 \text{ \AA}$  and  $u_{eq}^{LDA} = 0.2305$ , while the G-VFF results are  $a_{eq}^{G-VFF} = 5.8611 \text{ \AA}$  and  $u_{eq}^{G-VFF} = 0.2305$ . In comparison the original VFF yields  $a_{eq}^{VFF} = 5.8476 \text{ \AA}$  and  $u_{eq}^{VFF} = 0.2303$ .

## B The Empirical Pseudopotential Hamiltonian

We set up the single-particle Hamiltonian as

$$\hat{H} = -\frac{\beta}{2} \nabla^2 + \sum_{n\alpha} \hat{v}_\alpha(\mathbf{r} - \mathbf{R}_{n\alpha}) , \quad (6)$$

where  $\mathbf{R}_{n\alpha}$  is the G-VFF relaxed position of the  $n^{th}$  atom of type  $\alpha$ . Here  $\hat{v}_\alpha(\mathbf{r})$  is a screened empirical pseudopotential for atomic type  $\alpha$ . It contains a local part and a nonlocal, spin-orbit interaction part.

The local potential part is designed to include dependence on the local hydrostatic strain  $\text{Tr}(\epsilon)$ :

$$v_\alpha^{loc}(r; \epsilon) = v_\alpha^{eq}(r; 0)[1 + \gamma_\alpha \text{Tr}(\epsilon)] , \quad (7)$$

where the  $\gamma_\alpha$  is a fitting parameter. The zero strain potential  $v_\alpha^{eq}(r; 0)$  is expressed in reciprocal space  $\mathbf{q}$  as

$$v(\mathbf{q}) = a_0(q^2 - a_1)/[a_2 e^{a_3 q^2} - 1] . \quad (8)$$

The local hydrostatic strain  $\text{Tr}(\epsilon)$  for a given atom at  $\mathbf{R}$  is defined as  $\Omega_R/\Omega_0 - 1$ , where  $\Omega_R$  is the volume of the tetrahedron formed by the four atoms bonded to the atom at  $\mathbf{R}$ .  $\Omega_0$  is the volume of that tetrahedron in the unstrained condition. The need for explicit dependence of the atomic pseudopotential on strain in Eq.(7) results from the following: While the description in Eq.(6) of the total pseudopotential as a superposition of atomic potentials situated at specific sites,  $\{\mathbf{R}_{n\alpha}\}$ , does capture the correct local symmetries in the system, the absence of a self-consistent treatment of the Schrödinger equation deprives the potential from changing in response to strain. In the absence of a strain-dependent term, the volume dependence of the energy of the bulk valence band maximum is incorrect. While self-consistent descriptions show that the volume deformation potential  $a_v = dE_v/d\ln\Omega$  of the valence band maximum is *negative* for GaAs, GaSb, InAs, InSb and for all II-VI this qualitative behavior can not be obtained by a non-self-consistent calculation that lacks a strain dependent pseudopotential.

The nonlocal part of the potential describes the spin-orbit interaction,

$$H_{so} = \sum_{n\alpha} \hat{V}_{\alpha}^{so}(R_{n\alpha}) \quad (9)$$

$$\equiv \sum_{n\alpha} \sum_l V_{l,\alpha}^{so}(r - R_{n\alpha}) |l\rangle_{R_{n\alpha}} \mathbf{L} \cdot \mathbf{S} \langle l|_{R_{n\alpha}} ,$$

where  $|l\rangle_{R_{n\alpha}}$  is a projector of angular momentum  $l$  centered at  $R_{n\alpha}$ ,  $\mathbf{L}$  is the spatial angular momentum operator,  $\mathbf{S}$  is the Dirac spin operator, and  $V_{l,\alpha}^{so}(r)$  is a potential describing the spin-orbit interaction.

In Eq(6), the kinetic energy of the electrons has been scaled by a factor of  $\beta$ . The origin of this term is as follows: In an accurate description of the crystal band structure, such as the GW method[38], a general, spatially non-local potential,  $V(r, r')$ , is needed to describe the self-energy term. In the absence of such a term the occupied band width of an inhomogeneous electron gas is too large compared to the exact many-body result. To a first approximation, however, the leading effects of this non-local potential,  $V(r, r')$ , can be represented by scaling the kinetic energy. This can be seen by Fourier transforming  $V(r, r')$  in reciprocal space,  $q$ , then making a Taylor expansion of  $q$  about zero. We find that the introduction of such a kinetic energy scaling,  $\beta$  permits a simultaneous fit of both the effective masses and energy gaps. In this study, we fit  $\beta = 1.23$  for both GaAs and InAs.

The pseudopotential parameters in Eqs(7) and (8) were fitted to the bulk band structures, experimental deformation potentials and effective masses and first-principles calculations of the valence band offsets of of GaAs and InAs. The alloy bowing parameter for the GaInAs band gap (0.6 eV) is also fitted. The pseudopotential parameters are given in Table III and their fitted properties are given in Table I[39]. We see that unlike the LDA, here we accurately reproduce the bulk band gaps and the bulk effective masses. One significant difference in our parameter set, to that used in conventional k.p studies, is our choice of a negative magnitude for the valence band deformation potential,  $a_v$ , which we have obtained from LAPW calculations[40].

TABLE III: Parameters for the GaAs and InAs screened atomic pseudopotentials, in Eq.(7). This potential requires a plane wave cutoff of 5 Ryd.

Parameter	In	Ga	As (InAs)	As (GaAs)
$a_0$	644.13	432960	26.468	10.933
$a_1$	1.5126	1.7842	3.0313	3.0905
$a_2$	15.201	18880	1.2464	1.1040
$a_3$	0.35374	0.20810	0.42129	0.23304
$a_4$	2.1821	2.5639	0.0	0.0

The present InAs and GaAs pseudopotentials have been systematically improved relative to our previous InAs and GaAs potentials[35, 36, 41, 42, 43], although the functional form has remained the same. Firstly, the

pseudopotentials for InAs and GaAs used in Ref.[35, 42] did not include the spin-orbit interaction. In Refs.[41, 36, 43] we used potentials that included the spin-orbit interaction, but were not able to simultaneously, accurately fit the electron effective and the zone center band gap, due to the lack of the above  $\beta$  parameter. The potential used here is identical to that used in Refs.[42, 32].

### C Calculating the single particle eigenstates

One could use a straight forward expansion of the single particle wavefunctions in a plane wave basis set, as we have previously done in Refs.[37, 36, 35]. However, as was shown in Refs.[42, 32, 44], a more economical representation is to use the Linear Combination of Bulk Bands (LCBB) method[42, 32, 44]. Within the LCBB the eigenstates of the pseudopotential Hamiltonian are expanded in a basis of bulk Bloch orbitals

$$\psi_i(\mathbf{r}) = \sum_s \sum_{n,k} c_{s,n,k}^{(i)} u_{s,n,k}(\mathbf{r}) e^{i\mathbf{k}\cdot\mathbf{r}} , \quad (10)$$

where  $u_{s,n,k}(\mathbf{r})$  is the cell periodic part of the bulk Bloch wavefunction for structure,  $s$ , at the  $n^{th}$  band and the  $k^{th}$  k-point,  $k$ . These states form a physically more intuitive basis than traditional plane waves therefore the number of bands and k-points can be significantly reduced to keep only the physically important bands and k-points (around the  $\Gamma$  point in this case). This method was recently generalized to strained semiconductor heterostructure systems[42] and to include to spin-orbit interaction[43]. In this paper use an LCBB basis derived from four structures,  $s$ . These structures are (i) unstrained, bulk InAs at zero pressure, (ii) unstrained, bulk GaAs at zero pressure, (iii) bulk InAs subjected to the strain value in the center of the InAs dot, and (iv) bulk InAs subjected to the strain value at the tip of the InAs dot. By interpolating the strain profile between these four structures, the basis is able to accurately describe all the strain in the system. The wavevectors,  $\{k\}$ , used here include all allowed values within  $16\pi/L$  of the zone center, where  $L$  is the supercell size. For calculations of electron states, the band indices,  $n$ , include only the band around the  $\Gamma_{1c}$  point. For the hole states we also include the three bands around the  $\Gamma_{15v}$  point. This basis set produces single particle energies that are converged with respect to basis size, to within 1 meV.

### D Constructing the energies of different electronic configurations

Using screened Hartree Fock theory, the energy associated with loading  $N$  electrons into a quantum dot can be expressed[45] as

$$E_N = \sum_i (\epsilon_i + \Sigma_i^{pol}) n_i + \sum_{i < j} (J_{ij}^{ee} - K_{ij}^{ee}) n_i n_j , \quad (11)$$

where  $\epsilon_i$  are the single-particle energies and  $\Sigma_i^{pol}$  are the polarization self-energies of the  $i^{th}$  electron state,  $J_{ij}^{ee}$  and  $K_{ij}^{ee}$  are the direct and exchange Coulomb integrals between the  $i^{th}$  and  $j^{th}$  electronic states and  $n_i$  are the occupation numbers ( $\sum_i n_i = N$ ). As shown in Ref.[45], for free standing, colloidal quantum dots the dielectric constant inside the dot is dramatically different to that outside (vacuum) and hence the polarization self-energy,  $\Sigma_i^{pol}$ , is very significant ( $\sim 1$  eV). For self assembled InAs dots embedded in GaAs, the dielectric constants of InAs and GaAs are similar ( $\epsilon_\infty = 12.3, 10.6$ ) and we calculate this term as  $\sim 1$  meV, and hence we choose to neglect it here. The direct and exchange Coulomb energies, are defined as

$$J_{ij} = \int \int \frac{|\psi_i(\mathbf{r}_1)|^2 |\psi_j(\mathbf{r}_2)|^2}{\bar{\epsilon}(\mathbf{r}_1 - \mathbf{r}_2) |\mathbf{r}_1 - \mathbf{r}_2|} d\mathbf{r}_1 d\mathbf{r}_2$$

$$K_{ij} = \int \int \frac{\psi_i^*(\mathbf{r}_1) \psi_i(\mathbf{r}_2) \psi_j^*(\mathbf{r}_2) \psi_j(\mathbf{r}_1)}{\bar{\epsilon}(\mathbf{r}_1 - \mathbf{r}_2) |\mathbf{r}_1 - \mathbf{r}_2|} d\mathbf{r}_1 d\mathbf{r}_2 \quad (12)$$

where  $\bar{\epsilon}$  is a phenomenological, screened dielectric function[41] containing a Thomas Fermi electronic component and an ionic component from Ref.[46]. Our exchange automatically includes both short and long range components.

Denoting electron levels as  $e_0, e_1, e_2\dots$ , hole levels as  $h_0, h_1, h_2\dots$  and the number of electrons and holes as  $N$  and  $M$ , the total energy,  $E_{MN}$ , is

$$E_{MN} = \sum_i -\epsilon_{h_i} m_i + \sum_{i < j} (J_{ij}^{hh} - K_{ij}^{hh}) m_i m_j$$

$$+ \sum_i \epsilon_{e_i} n_i + \sum_{i < j} (J_{ij}^{ee} - K_{ij}^{ee}) n_i n_j$$

$$- \sum_{ij} (J_{ij}^{eh} - K_{ij}^{eh}) n_i m_j , \quad (13)$$

where  $n_i$  and  $m_i$  are the electron and hole occupation numbers respectively and  $\sum_i n_i = N$  and  $\sum_i m_i = M$ . Using Eq.(13), in the strong confinement regime where kinetic energy effects dominate over the effects of exchange and correlation, an exciton involving electrons excited from hole state  $i$  to electron state  $j$  can be expressed as

$$E_{ij}^{exciton} = (\epsilon_{e_j} - \epsilon_{h_i}) - J_{ji}^{eh} + K_{ji}^{eh} \delta_{S,0} . \quad (14)$$

To study charged dots, if one assumes the electron states are occupied in order of increasing energy (Aufbau principle), the total energy of a dot charged with  $N$  electrons,  $E_{0N}$ , is

$$E_{00} [e_0^0] = 0$$

$$E_{01} [e_0^1] = \epsilon_{e_0}$$

$$E_{02} [e_0^2] = 2\epsilon_{e_0} + J_{e_0, e_0}$$

$$E_{03} [e_0^2 e_1^1] = (2\epsilon_{e_0} + \epsilon_{e_1}) + [J_{e_0, e_0} + 2J_{e_0, e_1}] - K_{e_0, e_1}$$

$$E_{04} [e_0^2 e_1^2] = (2\epsilon_{e_0} + 2\epsilon_{e_1}) + [J_{e_0, e_0} + J_{e_1, e_1} + 4J_{e_0, e_1}]$$

$$- 2K_{e_0, e_1} . \quad (15)$$

As indicated in section II, our wavefunctions,  $\{\psi_i\}$ , are not iterated to self-consistency. This affects the magnitude of the direct and exchange Coulomb integrals. We have previously examined the accuracy of this perturbative treatment for colloidal InAs dots by comparing the non-self-consistent Coulomb energy with that obtained self consistently[47]. The differences were negligible.

### E Quantum well tests

To test the above methods, we first calculated the energy levels in a quantum well, and compared the results with experiment. In Fig. 1(a), we compare the calculated electron-heavy hole transition energies for a 96 Å  $\text{In}_{0.24}\text{Ga}_{0.76}\text{As}$  quantum well inside a GaAs matrix. The peaks in the experimental spectra occur[48] at 1.275, 1.395 and 1.538 eV. Our calculated transitions occur at 1.290, 1.404 and 1.545 eV respectively. Figure 1(b) compares the band gap of a  $\text{In}_{0.22}\text{Ga}_{0.78}\text{As}$  quantum well as a function of its thickness. The measured band gaps[49] for quantum wells with thicknesses of 6 and 18 ML are 1.458 and 1.351 eV. Our calculated values are 1.466 and 1.366 eV.

### IV. PHYSICAL QUANTITIES TO COMPARE WITH EXPERIMENT

The quantities we use to characterize the electronic structure are illustrated in Fig. 2 which shows a schematic layout of the electron and hole single-particle energy levels in a quantum dot. Assuming that all levels are spatially nondegenerate (thus having only spin degeneracy), we mark the electron levels as  $e_0, e_1, e_2\dots$  and the hole levels as  $h_0, h_1, h_2$ . The level  $e_0$  is sometimes called “s-like”, whereas  $e_1$  and  $e_2$  are called “p-like”, and  $e_3$  and  $e_4$  are called “d-like”. Since the GaAs environment of the InAs dots is largely unstrained, it is convenient to set as a reference energy the VBM of GaAs as  $E = 0$ , and the CBM of GaAs as  $E = 1520$  meV. All energy levels can be referenced with respect to these band edges. For the *electron levels*, the quantities that we consider are:

- (i) The number of dot-confined electron states,  $N_e$ .
- (ii) The spacing  $\delta_{sp} = \epsilon_{e_1} - \epsilon_{e_0}$  between “s-like” and “p-like” electron states.
- (iii) The splitting  $\delta_{pp} = \epsilon_{e_2} - \epsilon_{e_1}$  between the “p-like” electron states.
- (iv) The spacing  $\delta_{pd} = \epsilon_{e_3} - \epsilon_{e_2}$  between “p-like” and “d-like” electron states.
- (v) The “binding energy” of the first electron level,  $e_0$ , with respect to the GaAs conduction band minimum,  $\Delta E(e) = E_{\text{GaAs, CBM}} - \epsilon_{e_0}$ .
- (vi) The position of the bottom of the band for the 2D InAs “wetting layer” (WL) with respect to the GaAs CBM,  $\Delta E_{WL}^{(e)} = E_{\text{GaAs, CBM}} - E_{WL}^{(e)}$ .

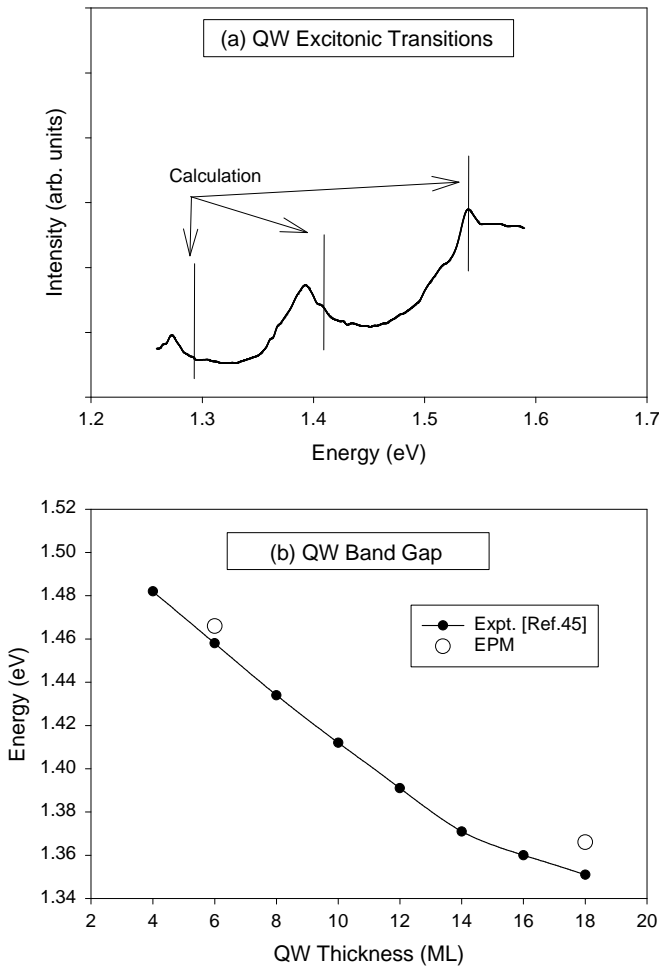


FIG. 1: (a) A comparison of EPM calculated and measured electron to heavy hole transition energies in a 96 Å In<sub>0.24</sub>Ga<sub>0.76</sub>As quantum well embedded inside a GaAs matrix. The vertical lines mark the positions of the EPM calculated transitions. (b) The calculated band gap of an In<sub>0.22</sub>Ga<sub>0.78</sub>As quantum well as a function of its thickness.

(vii) Inter-electron direct  $J_{e_i, e_j}^{ee}$  and exchange  $K_{e_i, e_j}^{ee}$  Coulomb energies.

For the *hole levels* we consider are:

- The number,  $N_h$ , of dot-confined hole states.
- The intra-band spacings of the hole levels,  $\delta_{ij}^{(h)} = \epsilon_{h_j} - \epsilon_{h_i}$ .
- The “binding energy” of the first hole level,  $h_0$ , with respect to the GaAs valence band maximum,  $-\Delta E(h) = E_{GaAs, VBM} + \epsilon_{h_0}$ .
- The position of the top of the band for the 2D InAs “wetting layer” (WL) with respect to the GaAs VBM,  $\Delta E_{WL}^{(h)} = -E_{GaAs, VBM} + E_{WL}^{(h)}$ .
- Inter-hole direct  $J_{h_i, h_j}^{hh}$  and exchange  $K_{h_i, h_j}^{hh}$  Coulomb energies.

Finally, for the *recombination of electrons and holes*, we consider:

(i) The excitonic energies,  $E_{ij}^{exciton}$ , as defined in Eq.(14). By subtracting calculated values for the single particle energies  $\epsilon_{e_j}$  and  $\epsilon_{h_i}$  from measured optical excitation energies one can estimate the electron-hole direct Coulomb energies  $J_{h_i e_j}$ .

(ii) The ratio of absorption intensities for light polarized along [110] and [1̄10] directions, defined as

$$\lambda = \frac{P_{[110]}}{P_{[1\bar{1}0]}} = \frac{\langle \psi_{e_0} | r_{[110]} | \psi_{h_0} \rangle^2}{\langle \psi_{e_0} | r_{[1\bar{1}0]} | \psi_{h_0} \rangle^2} . \quad (16)$$

This ratio can deviate from unity due to three reasons; (a) The dots has different dimensions in the [110] and [1̄10] directions. We refer to this as the the “geometric factor”. (b) The atomistic zincblende symmetry makes the two directions symmetry inequivalent even if the lengths along the two directions are equal. We refer to this as the “atomic symmetry factor”. One manifestation of this affect is that if the strain is calculated atomistically, it is different in the two directions even in the absence of a geometric factor[34]. (c) A piezoelectric field that breaks the symmetry. Previous studies[16] have shown that this effect is negligible in InAs/GaAs dots so we will neglect it here. k.p calculations neglect the “atomic symmetry” factor (except for the small effect of strain asymmetry), but retain the “geometric factor”. Pseudopotential calculations retain both effects. For example, in a *square* based pyramid (where by definition the “geometric factor” does not contribute), k.p produces  $\lambda = 1$ , while pseudopotential theory gives  $\lambda = 1.2$  (see Table V). This shows that there is not a simple mapping from dot shape to polarization anisotropy,  $\lambda$ .

(iii) Excitonic dipole: As the center of the electron and hole wavefunctions do not exactly coincide with each other, it is possible that an exciton will exhibit a detectable dipole moment,

$$d_{h_i, e_j} = \langle \psi_{h_i} | \hat{r} | \psi_{e_j} \rangle - \langle \psi_{e_j} | \hat{r} | \psi_{h_i} \rangle . \quad (17)$$

The quantities defined above characterize the electronic structure. Next, in section V, we will next provide all of these quantities from our calculations, and then in section VI we will extract measured values of these quantities from the available experiments.

## V. THEORETICAL RESULTS

The electronic structure of a series of GaInAs/GaAs self-assembled quantum dots was calculated using the methodology described in Section II. We have chosen to focus on the well established “lens shaped” dot geometry from Refs.[5, 6, 7, 8, 9, 10, 11, 12]. The shape of this dot is shown in Fig. 3. The profile is obtained by selecting the section of a pure InAs sphere that yields a circular base with diameter 252 Å and a height of 35 Å. The main experimental uncertainty about this dot is the composition profile. It is not known if the dots are pure

Fig. 2 Williamson et. al.

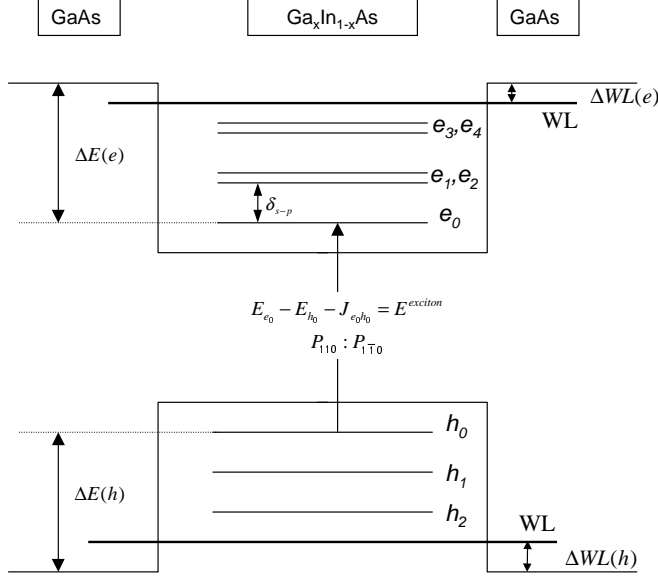


FIG. 2: Schematic single particle electron and hole energy levels for lens shaped, InAs quantum dots embedded within GaAs.

InAs or if Ga has diffused into the dots. For comparison, we also calculate the electronic structure of a square based InAs pyramid with a base of 113Å and a height of 56Å. This is not believed to be a realistic geometry, however, it has been used as a benchmark for many previous theoretical calculations[32, 35, 36, 50, 51] and we include it here for comparison purposes. In the following sections these two geometries will be referred to as the “lens” and the “pyramid”. The results of our calculations are shown in Table V and Fig. 4.

### A Confined electron states

Figure 4 shows the calculated square of the envelope function for the electron states in the pyramidal and lens shaped InAs/GaAs quantum dots. For the lens shaped dot, the electron states can be approximately interpreted as eigenstates of the  $\hat{L}_z$  operator[1]. Here we plot only the first 6 bound states corresponding to  $l_z = 0, \pm 1$  and  $\pm 2$ . The first state  $e_0$ , has  $l_z = 0$  and is commonly described as  $s$ -like as it has no nodes. The  $e_1$  and  $e_2$  states have  $l_z = \pm 1$ , and are  $p$ -like with nodal planes  $(110)$  and  $(\bar{1}\bar{1}0)$ . The  $e_3$ ,  $e_4$  and  $e_5$  states have  $l_z = \pm 2$  and 0 respectively and are commonly described as  $d_{x^2-y^2}$ ,  $d_{xy}$  and  $2s$  respectively. Due to the underlying zincblende atomistic structure, the  $C_\infty$  symmetry is reduced to  $C_{2v}$ . Hence, the  $e_0$  to  $e_5$  states correspond to the  $a_1, b_1, b_2, a_1, a_2$  and  $a_1$  irreducible representations of the  $C_{2v}$  group, rather than eigenstates of  $\hat{L}_z$ . This allows states  $e_0, e_3$  and  $e_5$  to couple. This coupling is evident, for example, in the

Fig. 3 Williamson et. al.

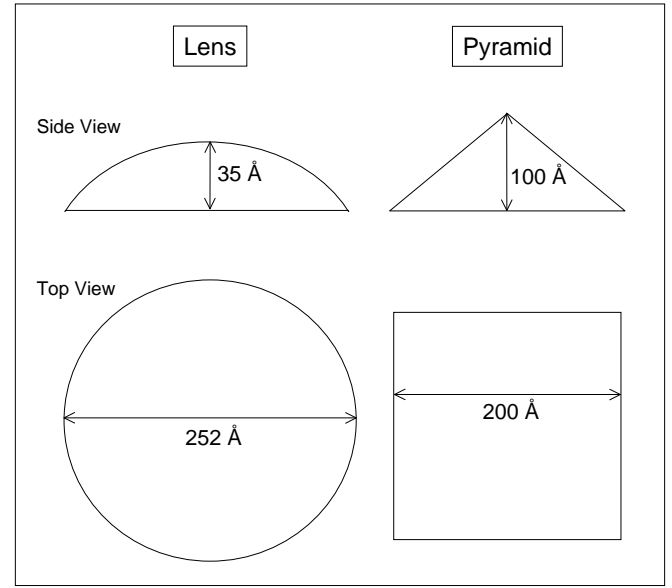


FIG. 3: Assumed model geometry of the lens and pyramidal shaped quantum dots.

larger charge density along  $[110]$  compared to  $[1\bar{1}0]$  in the  $e_3$  state, due to its coupling with  $e_1$ . The observable effect of this  $C_{2v}$  symmetry is to split the  $e_1$  and  $e_2$   $p$ -states,  $\delta_{pp}$ , and the  $e_3$  and  $e_4$   $d$ -states,  $\delta_{dd}$ . The alignment of the  $e_1$  and  $e_2$   $p$ -states states along the  $[110]$  and  $[1\bar{1}0]$  directions also results from the underlying zincblende lattice structure. Note, this analysis neglects the effects of the spin-orbit interaction which reduces the  $C_{2v}$  group to a double group with the same single representation for all the states. In our calculations the spin-orbit interaction is included, but it produces no significant effects for the electron states.

The electron states in the pyramidal dot also belong to the  $C_{2v}$  group and show a one-to-one correspondence with those in the lens shaped dot. However, there are only 5 bound states in the pyramidal dot due to its smaller size. Here we define an electron state as bound if its energy is below that of the unstrained, bulk GaAs conduction band edge.

The calculated values of the  $s$ - $p$  and  $p$ - $d$  energy spacings,  $\delta_{sp}$ , and,  $\delta_{pd}$ , for the lens and pyramidal shaped dots are 65 and 68 meV and 108 and 64 meV respectively. The splitting of the two  $p$  states,  $\delta_{pp} = e_2 - e_1$  are 2 and 26 meV respectively. The calculated values of the electron binding energy,  $\Delta E(e)$ , are 271 and 171 meV respectively. The electron-electron direct Coulomb energies,  $J_{e_0e_0}^{ee}$ ,  $J_{e_1e_1}^{ee}$  and  $J_{e_0e_1}^{ee}$  in the lens and pyramidal dots are calculated as 32, 25 and 25 meV and 40, 35 and 36 respectively. On applying a magnetic field in the growth direction, we calculate an increase in the splitting of the two  $p$  states ( $e_2 - e_1$ ) in the lens shaped dot from 2

to 20 meV. Details of this magnetic field calculation will be given in a future publication[52]. Finally, the energy of the electron wetting layer level,  $\Delta E_{WL}^{(e)}$ , with thicknesses of 1 and 2 ML is 15 and 24 meV below the CBM of unstrained bulk GaAs.

## B Confined hole states

Figure 4 shows calculated wavefunctions squared for the hole states in pyramidal and lens shaped InAs/GaAs quantum dots. Unlike the electron states, the hole states cannot be approximated by the solutions of a single band Hamiltonian. Instead there is a strong mixing between the original bulk Bloch states with  $\Gamma_{8v}$  and  $\Gamma_{7v}$  symmetry. The larger effective mass for holes results in a reduced quantum confinement of the hole states and consequently many more bound hole states. Only the 6 bound hole states with the highest energy are shown in Figure 4.

The calculated values of the  $h_0-h_1$ ,  $h_1-h_2$  and  $h_2-h_3$  hole level spacings for the pyramidal and lens shaped dots are 8,7 and 6 meV and 15, 20 and 1 meV respectively. The calculated hole binding energies,  $\Delta E(e)$ , are 194 and 198 meV. We calculate the highest energy hole level in pure InAs wetting layers,  $\Delta E_{WL}^{(h)}$ , with thicknesses of 1 and 2 ML to reside 30 and 50 meV above the VBM of unstrained bulk GaAs. The hole-hole Coulomb energies,  $J_{h_0 h_0}^{hh}$ , are 25 and 31 meV.

## C Electron-hole excitonic recombination

Figure 5 shows our calculated single exciton absorption spectrum for a pure InAs, lens shaped dot with a base of 252 Å and a height of 35 Å. The energies of each of the absorption peaks are calculated from Eq.(14). The ratios of the dipole matrix elements for light polarized along [110] and [1 $\bar{1}$ 0] are calculated from Eq.(16). Figure 5, illustrates that, for a lens shaped dot, both the conventional  $e_i \rightarrow h_i$  transitions and additional,  $e_1-h_2, e_2-h_1, e_3-h_4$  and  $e_4-h_3$  transitions are strongly allowed. The ratio of the polarization anisotropies,  $\lambda$ , are shown in Table IV. As a result of the circular symmetry of the lens shaped dot, we calculate a polarization ratio of  $\lambda = 1.03$  for the  $e_0 - h_0$  transition. This value is in contrast to that calculated value for a pyramidal dot of  $\lambda = 1.2$ [43]. For the higher angular momentum transitions we find larger deviations from unity. The magnitude of the ratios, follows the polarization of the wavefunctions shown in Fig. 4. For example we find ratios greater and then less than unity for the  $e_1 - h_1$  and  $e_2 - h_2$  transitions, as reflected by the elongations of the  $e_1, h_1$  and  $e_2, h_2$  wavefunctions along the [110] and [1 $\bar{1}$ 0] directions.

We calculate ground state electron-hole direct Coulomb energies,  $J_{e_0 h_0}^{eh}$ , of 37 and 31 meV in the lens shaped and pyramidal dots. The calculated ground state electron-hole exchange energies,  $K_{e_0 h_0}^{eh}$  are an order of magnitude smaller, with values of 3 and 0.2 meV. These

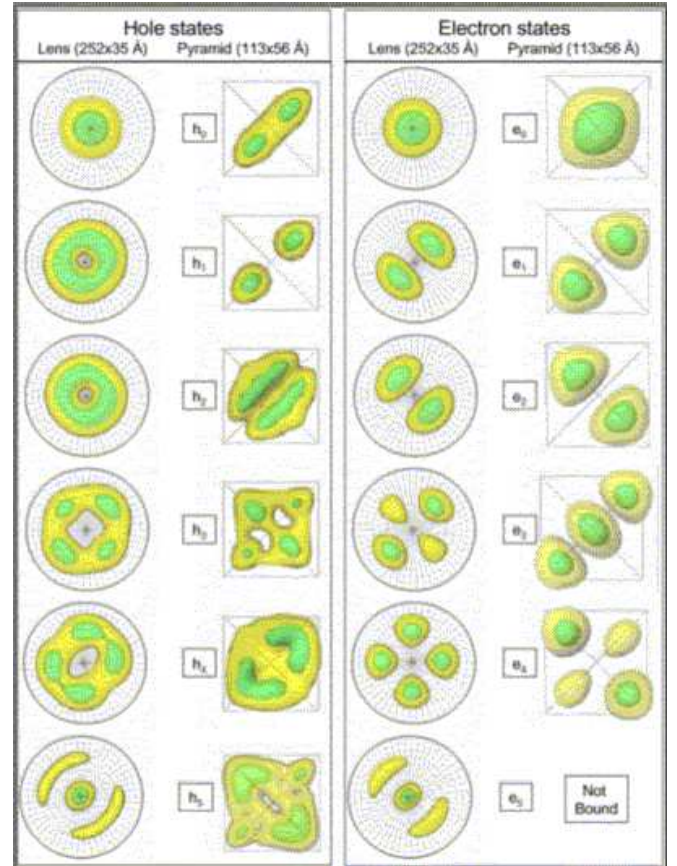


FIG. 4: Top view of the calculated electron and hole wavefunctions squared for lens and pyramidal shaped InAs quantum dots embedded in GaAs, with bases of 252 and 113 Å and heights of 25 and 56 Å. The yellow and green isosurfaces represent 20 and 60 % of the maximum charge density.

yield excitonic band gaps of 1.03 and 1.12 respectively. The calculated polarization anisotropy ratios [Eq.(16)] for light polarized along [110] and [1 $\bar{1}$ 0] directions are  $\lambda = 1.03$  and 1.20 for the lens and pyramidal shapes respectively. The calculated excitonic dipoles [Eq.(17)] are -3.1 and 0.16 Å respectively. A positive dipole is defined as the center of the hole wavefunction being located above the center of the electron wavefunction.

## VI. ANALYSIS OF PERTINENT EXPERIMENTAL MEASUREMENTS

### A The intra-band $s-p$ and $p-d$ electron energy spacings

Measurements of the spacing between the  $e_0$  and  $e_1$  like electron levels ( $s$ -like and  $p$ -like) are based on infra red absorption. For the lens shaped dots, Fricke *et. al.*[7] load electrons into the dots by growing a sample consisting of a n-type doped layer, a tunneling barrier,

Fig 5. Williamson *et. al.*TABLE IV: Calculated polarization anisotropy,  $\lambda_{P_{110} : P_{1\bar{1}0}}$ , for lens shaped and pyramidal  $\text{Ga}_x\text{In}_{1-x}$  quantum dots embedded within GaAs.

Geometry	Lens	Pyran
% Ga at base,tip,average	252x35 Å	200x100
$e_0 - h_0$	1.03	1.20
$e_1 - h_1$	0.82	2.40
$e_2 - h_2$	1.27	0.52
$e_3 - h_3$	0.73	4.26
$e_4 - h_4$	1.23	0.65

a layer of InAs/GaAs lens shaped dots, a GaAs sp<sub>2</sub> and a GaAs/AlAs short period superlattice (SPS). applying a voltage between the n-doped layer at the bottom of the sample and a Cr contact grown on top of the SPS, electrons are attracted from the n-doped layer into the InAs dots. Infra-red photons were used to excite electrons from the occupied  $e_0$  level into the  $e_1$  level. Neglecting the small exchange energy, the energy differences for the  $e_1 - e_0$  excitations when 1 and 2 electrons are present in the dot are

$$E_{01}[e_1^1] - E_{01}[e_0^1] = (\epsilon_{e_1} - \epsilon_{e_0})$$

$$E_{02}[e_0^1 e_1^1] - E_{02}[e_0^2] = (\epsilon_{e_1} - \epsilon_{e_0}) + [J_{e_1, e_0}^{ee} - J_{e_0, e_0}^{ee}]$$

The first of these energy differences yields a direct measurement of the  $s - p$  energy spacing,  $\delta_{sp}$ , of 49.1 meV. The second energy difference was measured at 50.1 meV. Drexler *et. al.*[5] also used infra-red transmission spectroscopy to measure the energy spacing,  $\delta_{sp} = 41$  meV. Pan *et. al.*[21, 24] have also performed infra-red absorption measurements on truncated pyramidal dots with a base of 180 Å and a height of  $\sim 60$  Å. In these experiments, no gate voltage is applied, and therefore the excitations take place from the ground state of the samples,  $E_{00}$ . They observe multiple infra-red absorption peaks between 89 and 103 meV. These could be associated either with the  $s-p$  spacing of the electron levels or spacings of the hole states (see below).

Itskevich *et. al.*[19] perform high power PL measurements of pyramidal dots with a base of 150 Å and a height of 30 Å. This high power excitation is able to simultaneously load multiple excitons into the dots. Due to state filling, these multiple excitons will occupy ground state ( $e_0, h_0$ ) and higher ( $e_1, e_2, h_0, h_1, h_2$ ) single particle levels. Therefore the PL measurements are able to simultaneously measure recombination between electrons occupying the  $e_0, e_1, e_2$  and  $e_3$  levels with holes in the  $h_0, h_1, h_2$  and  $h_3$  levels. In general, to describe the total energy differences associated with decay from  $N$  to  $N - 1$  excitons occupying a dot requires a treatment that includes the exchange and correlation between multiple occupational configurations of the  $N$  and  $N - 1$  excitonic states. Such a configurational interaction (CI) approach has previously been considered for model parabolic dots[1] and will be discussed for realistic dots in a future publication[53]. For the purposes of this

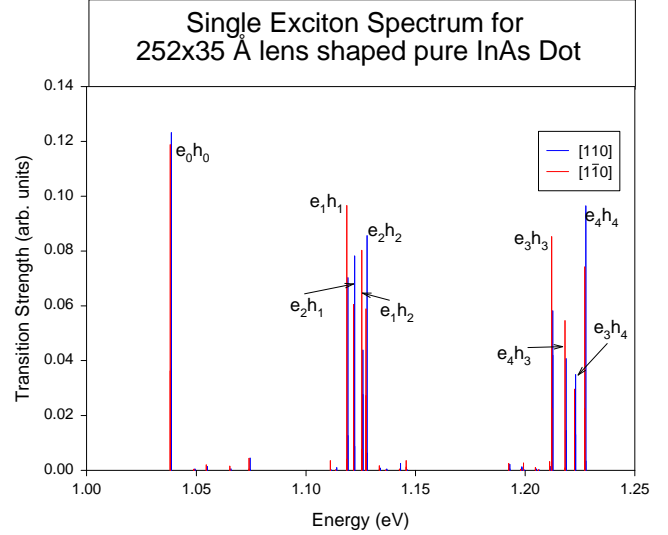


FIG. 5: The single exciton absorption spectrum for a pure InAs, lens shaped dot with a base of 252 Å and a height of 35 Å. The absorption peaks are calculated from Eq.(14). The ratios of the dipole matrix elements for light polarized along [110] and [1 $\bar{1}$ 0] are calculated from Eq.(16).

discussion, we limit ourselves to discussing the energy differences associated with the lowest energy configurations on the  $N$  exciton state, i.e. those predicted by the Aufbau principle. Within this approximation, the peaks in the high power, PL spectra can be interpreted as corresponding to [see Eq.(15) where exchange is neglected]

$$\begin{aligned}
 \text{Peak 1: } & E_{11}[h_0^1 e_0^1] - E_{00} = (\epsilon_{e_0} - \epsilon_{h_0}) - J_{e_0, h_0}^{eh} \\
 \text{Peak 2: } & E_{33}[h_0^2 h_1^1 e_0^2 e_1^1] - E_{22}[h_0^2 e_0^2] = (\epsilon_{e_1} - \epsilon_{h_1}) - J_{e_1, h_1}^{eh} \\
 & + 2[-J_{e_1, h_0}^{eh} - J_{e_0, h_1}^{eh} + J_{e_1, e_0}^{ee} + J_{h_1, h_0}^{hh}] \\
 \text{Peak 3: } & E_{77}[h_0^2 h_1^2 h_2^1 h_3^1 e_0^2 e_1^2 e_2^1] - E_{66}[h_0^2 h_1^2 h_2^2 e_0^2 e_1^2 e_2^2] \\
 & = (\epsilon_{e_3} - \epsilon_{h_3}) - J_{e_3, h_3}^{eh} \\
 & + 2 \sum_{i=0}^2 [-J_{e_3, h_i}^{eh} - J_{e_i, h_3}^{eh} + J_{e_3, e_i}^{ee} + J_{h_3, h_i}^{hh}] \quad .(19)
 \end{aligned}$$

Note, peak 3 is not assigned to a recombination from  $e_2$  to  $h_2$  as this is almost degenerate with peak 2. Itskevich *et. al.* assume that (i) the Coulomb integrals in the square brackets on the right hand side of Eq.(19) cancel, (ii) that  $J_{e_0, h_0}^{eh} = J_{e_1, h_1}^{eh} = J_{e_3, h_3}^{eh}$ , and (iii) that the hole spacings,  $\delta_{h_0 h_1}, \delta_{h_1 h_2}$ , are small compared to the electron level spacings. With these assumptions the spacings between peaks 1 and 2 and peaks 2 and 3 can be assigned to the  $s-p$  and  $p-d$  energy spacings. They find spacings  $\delta_{sp}$  and  $\delta_{pd}$  of 75 and 80 meV respectively. Our calcula-

tions suggest that assumptions (i), (ii) and (iii) probably introduce errors of  $\sim \pm 10$ ,  $\sim \pm 5$  and  $+10$  meV respectively. The neglect of exchange interactions in the above discussion also introduces an error of  $\sim \pm 5$  meV.

### B The intra-band electron $p$ level splitting

For the lens shaped dots, the Capacitance Voltage spectroscopy of Fricke *et. al.*[7] can be used to estimate the splitting of the  $p$  states,  $\delta_{pp}$ , by loading two electrons into the dot and exciting them using FIR spectroscopy. The relevant energy differences are

$$\begin{aligned} E_{02}[e_0^1 e_1^1] - E_{02}[e_0^2] &= (\epsilon_{e_1} - \epsilon_{e_0}) + [J_{e_1, e_0}^{ee} - J_{e_0, e_0}^{ee}] \\ E_{02}[e_0^1 e_2^1] - E_{02}[e_0^2] &= (\epsilon_{e_2} - \epsilon_{e_0}) + [J_{e_2, e_0}^{ee} - J_{e_0, e_0}^{ee}] \end{aligned} \quad (20)$$

By assuming  $J_{e_1, e_0}^{ee} = J_{e_2, e_0}^{ee}$ , the difference in the two above expressions yields the energy spacing  $\epsilon_{e_2} - \epsilon_{e_1}$ . They find a value of  $\sim 2$  meV. To measure the effect of a magnetic field on the splitting of the  $p$  states Fricke *et. al.*[7] use infra-red absorption to measure the above energy differences in an applied magnetic field. At a field of 15 Tesla they measure an energy spacing of 19 meV. More theoretically, Dekel *et. al.*[14] have demonstrated that one must assume a splitting of the  $p$  states to explain the number of multi-exciton levels observed in their single dot, micro PL measurements.

### C The intra-band hole energy spacings

There are currently no measurements available for the energy spacings between the hole states in the lens shaped dots. Itskevich *et. al.*[19] have performed high power PL measurements of dots estimated to be square based, truncated pyramids with a base of 150 Å and a height of 30 Å, under hydrostatic pressure to estimate hole level spacings. At hydrostatic pressures above 55 kbar, they measure the PL associated with transitions from the  $X_{1c}$ -state in the GaAs matrix to the  $h_0$  and  $h_1$  levels in the dots. They estimate a hole level spacing of  $\sim 15$  meV. However, the nature of the initial and final hole states is unclear.

Sauvage *et. al.*[22] use polarized photoinduced intraband absorption spectroscopy to measure the energy spacing between the lowest hole state,  $h_{000}$ , and the hole state with a single node in the growth direction,  $h_{001}$ . This corresponds to [see Eq.(15)]

$$\begin{aligned} E_{11}[h_{000}^1 e_0^1] - E_{11}[h_{001}^1 e_0^1] &= (\epsilon_{h_{001}} - \epsilon_{h_{000}}) \\ &+ [J_{e_0, h_{000}}^{eh} - J_{e_0, h_{001}}^{eh}] \end{aligned} \quad (21)$$

By assuming that  $J_{e_0, h_{000}}^{eh} = J_{e_0, h_{001}}^{eh}$  Sauvage *et. al.* estimate the  $h_{001} - h_{000}$  spacing to be  $\sim 120$  meV. Note  $h_{001}$  is almost certainly higher in energy than states with nodes perpendicular to the growth direction ( $h_{010}$  and  $h_{100}$ ) due

to the smaller dimension of the dot in the growth direction. Consequently, the energy difference  $h_{001} - h_{000}$  is not the spacing of the first two hole states  $h_0 - h_1$ .

Tang *et. al.*[54] measure activation energies for excitations from  $h_0$  and  $h_1$  to the hole wetting layer of 48 and 30 meV respectively, implying an  $h_0 - h_1$  spacing of  $\sim 18$  meV.

### D The electron and hole binding energies, $\Delta E(e)$ and $\Delta E(h)$

There have been no direct measurements of the electron or hole binding energy for lens shaped InAs dots. However, it has been measured in other dots by several groups using a range of techniques. Berryman *et. al.*[17] placed pyramidal InAs dots estimated to have a base of 100 Å and height of 15 Å in a p-n junction and measured the temperature dependence of the ac conductance as a function of frequency. These measurements predict a hole binding,  $\Delta E(h)$ , energy of  $\sim 240$  meV. When subtracted from the bulk GaAs band gap, this yields a value for the electron binding energy,  $\Delta E(e)$ , of  $\sim 60$  meV. The authors obtain similar results from temperature dependent Hall measurements of thermal hole trapping. Itskevich *et. al.*[18] measured the pressure at which PL measurements could detect a  $\Gamma$ -X crossing in pyramidal InAs/GaAs quantum dot samples. By extracting these PL measurements back to zero pressure they were able to extrapolate a value for the electron binding energy,  $\Delta E(e)$ , of  $\sim 50$  meV. Itskevich *et. al.*[19] also used high pressure PL to measure the energy difference between the  $X_{1c}$  level in bulk GaAs and the  $h_0$  level in the quantum dots. By extrapolating this value back to zero pressure, they predict a value for the hole binding energy,  $\Delta E(h)$ , of  $\sim 250$  meV. Brunkov *et. al.*[13] performed capacitance-voltage spectroscopy measurements, which when fitted to a capacitance model for their dot geometry predict an electron binding energy of 80 meV for dots with bases of 250 Å. Tang *et. al.*[54] measured the spacing of the electron wetting layer to both the GaAs CBM and the  $e_0$  level and hence deduced a value for the electron binding energy,  $\Delta E(e)$ , of  $\sim 80$  meV, for dots with an estimated base of 130 to 170 Å.

### E The position of the electron and hole wetting layer level

The presence of a distinct wetting layer signal in the PL spectra of a sample of self assembled quantum dots is the hallmark of a high quality sample. In samples where the wetting layer has “dissolved” due to the growth conditions, it is likely that the geometry and composition of the quantum dots will also have dramatically altered from their uncapped state.

In the lens shaped InAs dots Schmidt *et. al.*[10] observe PL emission from the ground state of the wetting

layer at 1.34 eV. Photovoltage measurements[10] on the same samples show a strong peak corresponding to absorption into the ground state of the wetting layer at 1.35 eV. There are currently no measurements available for the position of the individual electron and hole wetting layers in the lens shaped InAs/GaAs quantum dot samples. In Ref.[23] Sauvage *et. al.* grow lens shaped InAs dots with an estimated base of 150 Å and a height of 30 Å on a substrate that is n-doped with silicon. This n-doping loads electrons into the  $e_0$  state in the dot, which they excite into the wetting layer using infra-red excitation. In these samples they estimate the wetting layer to be 150 meV above the  $e_0$  level. In Ref. [22] Sauvage *et. al.* load electrons into the  $e_0$  state of similar dots using an optical interband pump. Subsequent infra-red absorption places the wetting layer 190 meV above the  $e_0$  state. Tang *et. al.*[54] measure thermal transfer of holes to the wetting layer, and obtain a spacing between the  $h_0$  level and the hole wetting layer,  $\Delta E_{WL}^{(e)}$  of  $\sim$ 48 meV. They also measure thermal transfer from an excited state, possibly involving  $h_1$ , which places the hole wetting layer  $\sim$ 30 meV below the  $h_1$  level.

## F The number of confined electron and hole states

The actual number of confined electron and hole states in a self assembled InAs/GaAs quantum dot depends on the size and composition of the dot. Early single band, effective mass calculations[50] for pure InAs pyramidal dots with a base of 120 Å and height 60 Å predicted only a single bound electron state and several bound hole states. Consequently, many experiments were then interpreted in this light. More accurate multi-band  $k.p$ [55, 56, 51] and pseudopotential[35, 36] calculations have predicted 5 or more bound electron states in the same dots.

The high power PL experiments of Itskevich *et. al.*[19] show the gradual disappearance of 5 peaks as a function of external pressure. This is interpreted as direct evidence for 5 confined electron levels in their samples. The single dot, multi-exciton measurements of Dekel *et. al.*[14] require the assumption of at least 3 bound electron states to explain their experimental spectra. Similarly, the capacitance-voltage spectroscopy of Fricke *et. al.*[7] shows two peaks corresponding to the capacitance of *s*-like states and the nearly degenerate *p*-like states, providing evidence for at least 3 bound electron states.

## G Electron and hole Coulomb and Exchange Interactions

By loading multiple electrons and holes into quantum dots it is possible to measure the Coulomb and exchange interactions between these additional electrons and holes. The magnitude of these interactions is a function of the shape of the electronic wavefunctions (see section II) and

provides an additional quantity to test the accuracy of theoretical models.

To study electron-electron interactions, Fricke *et. al.*[7] use the same experimental setup discussed in section VIA. From Eq.(15) we see the energy differences corresponding to the peaks in the Capacitance Voltage (CV) spectra associated with loading one and two electrons into the  $e_0$  level in the dots is

$$\begin{aligned} E_{01} [e_0^1] - E_{00} &= \epsilon_{e_0} \\ E_{02} [e_0^2] - E_{01} [e_0^1] &= \epsilon_{e_0} + J_{e_0, e_0}^{ee} . \end{aligned} \quad (22)$$

The electron-electron Coulomb interaction,  $J_{e_0, e_0}^{ee}$ , can therefore be directly measured as the splitting of these two CV peaks. They find a value of  $J_{e_0, e_0}^{ee} \sim$ 23 meV. From Eq.(18) we see that

$$J_{e_0, e_1}^{ee} = J_{e_0, e_0}^{ee} + (50.1 - 49.1) = 24 \text{ meV} . \quad (23)$$

Finally by fitting 4 equidistant bell curves to the CV spectra corresponding to loading 3,4,5 and 6 electrons into the dots, an approximate value for the charging energy between the *p* states,  $J_{e_1, e_1}^{ee}$ , of  $\sim$ 18 meV is obtained. From Eq.(15) we see that the spacing  $E_{04} - E_{03} = J_{e_1, e_1}^{ee} + 2J_{e_0, e_1}^{ee}$ , while  $E_{06} - E_{05} = 3J_{e_1, e_1}^{ee} + 2J_{e_0, e_1}^{ee}$  and hence the approximation of equidistant peaks will introduce some error into this estimate for  $J_{e_1, e_1}^{ee}$ .

## H Electron-hole excitonic recombination

To our knowledge there have so far been no measurements of the polarization anisotropy in the lens shaped dots discussed here. The polarization anisotropy for  $e_i - h_i$  excitonic recombination in InAs/GaAs was measured by Yang *et. al.*[15, 16], who find a ratio of  $\lambda_{e_0, h_0} = 1.2$  and  $\lambda_{e_2, h_2} = 1.3$  for InAs dots whose geometry is measured to be formed by four {136} faceted planes with bases ranging from 150 to 250 Å and a base to height ratio of 4:1. Yang *et. al.*[15, 16] have performed *k.p* calculations for this dot geometry, which include the “geometric factor” but not the “atomic symmetry factor” discussed in section IV. They find  $\lambda_{e_0, h_0} = 1.8$  and  $\lambda_{e_2, h_2} = 3.5$ . The authors suggest the *k.p* simulations of the measured polarization ratio can be used to deduce the geometric shape anisotropy. However, we demonstrate here that when the “atomic symmetry factor” is included an anisotropy of  $\lambda_{e_0, h_0} = 1.3$  is obtained even for a *square* based pyramid. Thus *k.p* simulations lacking the “atomic symmetry” factor can not be used to reliably deduce the geometric shape anisotropy.

To our knowledge there have so far been no measurements of the excitonic dipole in lens shaped InAs dots. Fry *et. al.*[20] used photocurrent spectroscopy within an applied electric field to measure the excitonic dipole moment,  $d_{h_i, e_j}$ , [Eq.(17)]. They find the center of the hole wavefunctions to be located  $\sim$ 4 Å above the center of the electron wavefunction (positive dipole). Fry *et. al.*[20] also perform single-band, effective mass calculations, in

an attempt to isolate the origin of this dipole. They predict that in the absence of alloying the dipole is  $-3 \text{ \AA}$ , i.e. the opposite sign, but a linear composition profile with  $\text{Ga}_{0.5}\text{In}_{0.5}\text{As}$  at the base and pure InAs at the top of a truncated pyramid with a base of  $155 \text{ \AA}$ , and height  $55 \text{ \AA}$ , reproduces the correct dipole of  $4 \text{ \AA}$ . They suggest that this alloying profile explains the observed dipole. We have repeated these calculations and confirm that, within a single-band model, such a composition profile causes both electrons and holes to move up in the dot compared to their positions in a pure InAs dot. The heavier effective mass of the holes, results in less kinetic energy associated with confinement at the top of the dot and hence the holes move up more than electrons on the introduction of Ga, producing the correct dipole. However, when we repeat these calculations in the more sophisticated, multi-band LCBB basis used here, we find significant heavy hole-light hole mixing in the  $h_0$  state, which acts to reduce the above effect and produce a smaller dipole of  $\sim 1 \text{ \AA}$ , in contradiction with experiment ( $+4 \text{ \AA}$ ). We therefore conclude that in a more complete calculation the shape and alloy profile postulated by Fry *et. al.*[20] does not produce the observed excitonic dipole.

## VII. COMPARISON OF EXPERIMENT AND THEORY

In Table V we show the results of our calculations for pure InAs, lens shaped quantum dots embedded within GaAs [column (a)]. Table V also shows the experimentally measured splittings of the electron levels, the electron-electron and electron-hole Coulomb energies, the magnetic field dependence and the excitonic band gap measured in Refs.[7] and [11]. The agreement between the measured energy level spacings, Coulomb energies and magnetic field response with our theoretical lens shaped model is generally good. Both the model and experiment find (i) a large spacing,  $\delta_{sp}$ , ( $\sim 50\text{-}60 \text{ meV}$ ) between the *s*-like  $e_0$  state and the *p*-like  $e_1$  state, (ii) a small spacing,  $\delta_{pp}$ , ( $\sim 3 \text{ meV}$ ) between the two *p*-like  $e_1$  and  $e_2$  states and (iii) a large spacing ( $\sim 55 \text{ meV}$ ) between the *p*-like  $e_2$  state and the *d*-like  $e_3$  state.

These electron level spacings are similar to those found for pyramidal quantum dots[35] (see Table V). However, in the pyramidal dot, the spacings of the two *p*-like and *d*-like states,  $\delta_{pp}, \delta_{dd}$ , is larger (26 and 23 meV) as a result of the lower  $C_{2v}$  symmetry of a zincblende pyramid. Both the model and experiment also find similar values for the Coulomb energies,  $J(e_0e_0)$  and  $J(e_0h_0)$  ( $\sim 25 \text{ meV}$ ).

The calculated hole binding energy of  $\Delta E(h) = 193 \text{ meV}$  is in good agreement with those of Berryman *et. al.*[17] ( $\sim 240 \text{ meV}$ ) and Itskevich *et. al.*[19] ( $\sim 250 \text{ meV}$ ). Our calculated electron binding energies,  $\Delta E(h)$ , are considerably larger (271 meV) than those of Berryman *et. al.*[17] ( $\sim 60 \text{ meV}$ ) and Tang *et. al.*[54] ( $\sim 80 \text{ meV}$ ). We attribute this difference to the larger size of our dots.

The assumption of a pure InAs dot also affects the comparison. The agreement improves when we include Ga in our dots (see section VII B).

The calculated electron-electron and electron-hole Coulomb energies are in reasonable agreement with those extracted from Refs.[7] and [11]. For the integrals  $J_{e_0e_0}^{ee}, J_{e_0e_1}^{ee}, J_{e_1e_1}^{ee}$  and  $J_{e_0h_0}^{eh}$  we calculate values of 31, 25, 25 and 37 respectively, compared to measured values of 23, 24, 18 and 33.3 meV

The calculated polarization anisotropies,  $\lambda$ , for the  $e_0 - h_0$  recombination in lens and pyramidal shaped, pure InAs dots are  $\lambda = 1.03$  and 1.2 respectively. A future measurement of this anisotropy ratio for lens shaped dots would provide an important piece of evidence for determining the detailed geometry of the dots.

In the lens shaped dot we find a difference in the average positions of the  $h_0$  and  $e_0$  states,  $d_{h_i, e_j}$ , of around  $1 \text{ \AA}$ . This is smaller than the value we calculate for a pyramidal quantum dot, where we find the hole approximately  $3.1 \text{ \AA}$  higher than the electron.

In summary, the assumed lens shaped geometry, with a pure InAs composition produces a good agreement with measured level splitting, Coulomb energies and magnetic field dependence. A closer inspection of the remaining differences reveals that the calculations systematically *overestimate* the splittings between the single particle electron levels ( $\delta_{sp}$ : 65 *vs.* 50 meV,  $\delta_{pd}$ : 68 *vs.* 48 meV) and *underestimates* the excitonic band gap (1032 *vs.* 1098 meV).

### A Pure InAs dots: The effects of shape and size

Focusing on the lens shape only, we examine the effect of changing the height and base of the assumed geometry. Calculations were performed on similar lens shaped, pure InAs dots where (i) the base of the dot was increased from  $252 \text{ \AA}$  to  $275 \text{ \AA}$ , while keeping the height fixed at  $35 \text{ \AA}$ , [column (b)] and (ii) the height of the dot was decreased from  $35 \text{ \AA}$  to  $25 \text{ \AA}$ , while keeping the base fixed at  $252 \text{ \AA}$ , [column (c)]. It shows that decreasing the height of the dot increases the quantum confinement and hence increases the splittings of the electron and hole levels ( $\delta_{sp}$ : from 65 to 69 meV and  $\delta_{h_0, h_1}$ : from 8 to 16 meV). Decreasing the height of the dot also acts to increase the excitonic band gap from 1032 to 1131 meV by pushing up the energy of the electron levels and pushing down the hole levels. Conversely, increasing the base of the dot decreases both the splittings of the single particle levels ( $\delta_{sp}$ : from 66 to 61 meV) and the band gap (1032 to 1016 eV). These small changes in the geometry of the lens shaped dot have only a small effect on electronic properties that depend on the shape of the wavefunctions. The electron-electron and electron-hole Coulomb energies remain relatively unchanged, the magnetic field induced splitting remain at 20 meV, the polarization anisotropy,  $\lambda$ , remains close to 1.0 and the excitonic dipole,  $d_{h_i, e_j}$ , remains negligible. In summary, reducing either the height or the base of

the dot increases quantum confinement effects and hence increases energy spacings and band gaps, while not significantly effecting the shape wavefunctions.

### B Interdiffused In(Ga)As/GaAs lens shaped dots

We next investigate the effect of changing the composition of the quantum dots, while keeping the geometry fixed. There have recently been several experiments[20, 25, 26] suggesting that a significant amount of Ga diffuses into the nominally pure InAs quantum dots during the growth process. We investigate two possible mechanisms for this Ga in-diffusion; (i) Ga diffuses into the dots during the growth process from all directions producing a dot with a uniform Ga composition  $\text{Ga}_x\text{In}_{1-x}\text{As}$ , and (ii) Ga diffuses up from the substrate, as suggested in Ref.[20]. To investigate the effects of these two methods of Ga in-diffusion on the electronic structure of the dots, we compare pure InAs dots embedded in GaAs with  $\text{Ga}_x\text{In}_{1-x}\text{As}$ , random alloy dots embedded in GaAs, where the Ga composition,  $x$ , (i) is fixed at 0.15, [column (d)] and (ii) varies linearly from 0.3 at the base to 0 at the top of the dot, [column (e)].

The electronic structure of these dots is compared in Table V. It shows that increasing the amount of Ga in the dots acts to decrease the electron level spacings ( $\delta_{sp}$ : from 65 to 58 and 64 meV for  $x = 0.15$  and  $x = 0.3$  to  $x = 0$  respectively). It also acts to increase the excitonic band gap from 1032 to 1080 and 1125 meV respectively. The electron binding energy,  $\Delta E(e)$ , is decreased by the in diffusion of Ga (from 271 to 209 and 192 meV), while the hole binding energy,  $\Delta E(h)$ , is relatively unaffected. This significant decrease in the electron binding energy considerably improves the agreement with experiments on other dot geometries[17, 54].

As with changing the size of the dots, we find that Ga in-diffusion has only a small effects on properties that depend on the shape of the wavefunctions. The calculated electron-electron and electron-hole Coulomb energies are almost unchanged, while the average separation of the electron and hole,  $d_{h_i,e_j}$ , increases from 0.16 to 0.5 and 1.2 Å and the polarization ratio,  $\lambda$ , and magnetic field response are also unchanged.

Table V shows that the dominant contribution to the increase in the excitonic band gap and reduction in electron binding energy, results mostly from an increase in the energy of the *electron* levels as the Ga composition is increased. This can be understood by considering the electronic properties of the bulk  $\text{Ga}_x\text{In}_{1-x}\text{As}$  random alloy. The unstrained valence band offset between GaAs and InAs is  $\sim 50$  meV[57], while the conduction band offset in  $\sim 1100$  meV and hence changing the Ga composition,  $x$ , has a large effect on the energy of the electron states and only a small effect on the hole states. In summary, the effect of Ga in-diffusion is to reduce the spacing of the electron levels while significantly increasing their energy and hence increasing the band gap. We find that

only the average Ga composition in the dots is important to their electronic properties. Whether this Ga is uniformly or linearly distributed throughout the dots has a negligible effect. Note, in Ref.[20] it is suggested that a linear composition profile is required to produce an excitonic dipole moment in agreement with that measured by stark experiments. For the lens shaped geometry discussed here there have so far been no such measurements of the dipole, but our calculations suggest that it should be small ( $\sim 1\text{\AA}$ ).

## VIII. DISCUSSION

The effects of changing the *geometry* of the lens shaped, pure InAs dots on the single particle energy levels can be qualitatively understood from single band, effective mass arguments. These predict that decreasing any dimension of the dot, increases the quantum confinement and hence the energy level spacings and the single particle band gap will increase. Note that as the dominant quantum confinement in these systems arises from the vertical confinement of the electron and hole wavefunctions, changing the height has a stronger effect of the energy levels than changing the base. In this case decreasing the height by 10 Å has a much stronger effect on the energy spacings and on the band gap than increasing the base by 23 Å.

As increasing(decreasing) the dimensions of the dot acts to decrease(increase) both the level spacings and the gap, it is clear that changing the dot geometry alone will not significantly improve the agreement with experiment as this requires a simultaneous *decrease* in the energy level splittings and *increase* in the band gap. However, Ga in-diffusion into the dots acts to *increase* the band gap of the dot while decreasing the energy level spacings. Table V shows that adopting a geometry with a base of 275 Å and a height of 35 Å and a uniform Ga composition of  $\text{Ga}_{0.15}\text{In}_{0.85}\text{As}$  produces the best fit to the measurements in Refs.[7] and [11].

In conclusion, our results strongly suggest that to obtain very accurate agreement between theoretical models and experimental measurements for lens shaped quantum dots, one needs to adopt a model of the quantum dot that includes some Ga in-diffusion within the quantum dot. When Ga in-diffusion is included, we obtain an excellent agreement between state of the art multi-band pseudopotential calculations and experiments for a wide range of electronic properties. We are able to predict most observable properties to an accuracy of  $\pm 5$  meV, which is sufficient to make predictions of both the geometry and composition of the dot samples.

**Acknowledgments** We thank J. Shumway and A. Franceschetti for many useful discussions and their comments on the manuscript. This work was supported DOE – Basic Energy Sciences, Division of Materials Science under contract No. DE-AC36-99GO10337.

## REFERENCES

[1] L. Jacak, P. Hawrylak, and A. Wojs, *Quantum Dots* (Springer, 1997).

[2] S. Gaponenko, *Optical Properties of Semiconductor Nanocrystals* (Cambridge University Press, 1998).

[3] A. Zunger, MRS Bulletin **23**, 35 (1998).

[4] L. Landin, M. Miller, M.-E. Pistol, C. Pryor, and L. Samuelson, Science **280**, 262 (1998).

[5] H. Drexler, D. Leonard, W. Hansen, J. Kotthaus, and P. Petroff, Phys. Rev. Lett. **73**, 2252 (1994).

[6] D. Medeiros-Ribeiro, G. a nd Leonard and P. Petroff, Appl. Phys. Lett. **66**, 1767 (1995).

[7] M. Fricke, A. Lorke, J. Kotthaus, G. Medeiros-Ribeiro, and P. Petroff, EuroPhys. Lett. **36**, 197 (1996).

[8] B. Miller, W. Hansen, S. Manus, R. Luyken, A. Lorke, J. Kotthaus, S. Huant, G. Medeiros-Ribeiro, and P. Petroff, Phys. Rev. B **56**, 6764 (1997).

[9] R. Warburton, C. Durr, K. Karrai, J. Kotthaus, G. Medeiros-Ribeiro, and P. Petroff, Phys. Rev. Lett. **79**, 5282 (1997).

[10] K. Schmidt, G. Medeiros-Ribeiro, J. Garcia, and P. Petroff, Appl. Phys. Lett **70**, 1727 (1997).

[11] R. Warburton, B. Miller, C. Durr, C. Bodefeld, K. Karrai, J. Kotthaus, G. Medeiros-Ribeiro, P. Petroff, and S. Huant, Phys. Rev. B **58**, 16221 (1998).

[12] K. Schmidt, G. Medeiros-Ribeiro, and P. Petroff, Phys. Rev. B **58**, 3597 (1998).

[13] P. Brunkov, A. Suvorova, N. Vert, A. Kovsh, A. Zhukov, A. Egorov, V. Ustinov, tsat-sul'nikov.a.F., N. Ledentsov, P. Kop'ev, and S. Konnikov, Semicond. **32**, 1096 (1998).

[14] E. Dekel, D. Gershoni, E. Ehrenfreund, D. Spektor, J. Garcia, and P. Petroff, Phys. Rev. Lett. **80**, 4991 (1998).

[15] W. Yang, H. Lee, , P. Sercel, and A. Norman, SPIE Photonics, **1**, 3325 (1999).

[16] W. Yang, H. Lee, J. Johnson, P. Sercel, and A. Norman, Phys. Rev. B (2000).

[17] K. Berryman, S. Lyon, and S. Mordechai, J. Vac Sci. Technol. B **15**(4), 1045 (1997).

[18] I. Itskevich, S. Lyapin, I. Troyan, P. Klipstein, L. Eaves, P. Main, and M. Henini, Phys. Rev. B **58**, R4250 (1998).

[19] I. Itskevich, M. Skolnick, D. . Mowbray, I. Troyan, S. Lyapin, L. Wilson, M. Steer, M. Hopkinson, L. Eaves, and P. Main, Phys. Rev. B **60**, R2185 (1999).

[20] P. Fry, I. Itskevich, D. Mowbray, M. Skolnick, J. Barker, E. O'Reilly, L. Wilson, I. Larkin, P. Maksym, M. Hopkinson, M. Al-Khafaji, J. David, *et al.*, Phys. Rev. Lett. **84**, 733 (2000).

[21] D. Pan, E. Towe, and S. Kennerly, Electronics Lett. **34**, 1019 (1998).

[22] S. Sauvage, P. Boucaud, T. Brunhes, A. Lemaitre, and J.-M. Gerard, Appl. Phys. Lett **71**, 2785 (1997).

[23] S. Sauvage, P. Boucaud, F. Julien, J.-M. Gerard, and V. Thierry-Mieg, Appl. Phys. Lett **71**, 2785 (1997).

[24] D. Pan, E. Towe, and S. Kennerly, Appl. Phys. Lett. **73**, 1937 (1998).

[25] T. Metzger, I. Kegel, R. Paniago, and J. Peisl, Private communication (1999).

[26] J. Garcia, G. Medeiros-Ribeiro, K. Schmidt, T. Ngo, F. Feng, A. Lorke, J. Kotthaus, and P. Petroff, Appl. Phys. Lett. **71**, 2014 (1997).

[27] M. Rubin, Medeiros-Ribeiro.G., J. O'Shea, M. Chin, E. Lee, P. Petroff, and V. Narayananmurti, Phys. Rev. Lett. **77**, 5268 (1996).

[28] D. Wood and A. Zunger, Phys. Rev. B **53**, 7949 (1996).

[29] H. Fu and A. Zunger, Phys. Rev. Lett. **80**, 5397 (1998).

[30] L.-W. Wang and A. Zunger, J. Phys. Chem. **102**, 6449 (1998).

[31] C. Pryor, Phys. Rev. B **57**, 7190 (1998).

[32] L.-W. Wang, A. Williamson, A. Zunger, H. Jiang, and J. Singh, Appl. Phys. Lett. **76**, 339 (2000).

[33] P. Keating, Phys. Rev. **145**, 637 (1966).

[34] C. Pryor, J. Kim, L.-W. Wang, A. Williamson, and A. Zunger, J. Appl. Phys. **83**, 2548 (1998).

[35] J. Kim, L.-W. Wang, and A. Zunger, Phys. Rev. B **57**, R9408 (1998).

[36] A. Williamson and A. Zunger, Phys. Rev. B **59**, 15819 (1999).

[37] A. Williamson and A. Zunger, Phys. Rev. B **57**, R4253 (1998).

[38] L. Hedin, J. Phys. C **11**, R489 (1999).

[39] Landolt and Borstein, *Numerical Data and Functional Relationships in Science and Technology, Volume 22, Subvolume a* (Springer-Verlag, Berlin, 1997).

[40] A. Franceschetti, S.-H. Wei, and A. Zunger, Phys. Rev. B **50**, 17797 (1994).

[41] A. Williamson and A. Zunger, Phys. Rev. B **58**, 6724 (1998).

[42] L.-W. Wang and A. Zunger, Phys. Rev. B **59**, 15806 (1999).

[43] L.-W. Wang, A. Williamson, and A. Zunger, Phys. Rev. B **xxx** (1999).

[44] L.-W. Wang, Franceschetti.A.F., and A. Zunger, Phys. Rev. Lett. **78**, 2819 (1997).

[45] A. Franceschetti, A. Williamson, and A. Zunger, J. Phys. Chem. (2000).

[46] H. Haken, Nuovo Cimento **10**, 1230 (1956).

[47] A. Franceschetti and A. Zunger, Phys. Rev. Lett. **78**, 915 (1997).

[48] D. Gershoni, F. Vandenberg, S. Chu, G. Temkin, T. Tanbun-Ek, and R. Logan, Phys. Rev. B. **40**, 10017 (1989).

[49] J. Laymarie, C. Monier, A. Vasson, A.-M. Vasson, M. Leroux, B. Courboules, N. Grandjean, C. De-paris, and J. Massies, Phys. Rev. B **51**, 13274 (1995).

[50] M. Grundmann, O. Stier, and D. Bimberg, Phys.

Rev. B **52**, 11969 (1995).

- [51] M. Cusak, P. Briddon, and M. Jaros, Phys. Rev. B **54**, 2300 (1996).
- [52] J. Shumway and A. Zunger, in preparation (2000).
- [53] A. Williamson and A. Zunger, In preparation (2000).
- [54] Y. Tang, D. Rich, I. Mukhametzhanov, P. Chen, and A. Hadhukar, J. Appl. Phys. **84**, 3342 (1998).
- [55] O. Stier, M. Grundman, and D. Bimberg, Phys. Rev. B **59**, 5688 (1999).
- [56] H. Jiang and J. Singh, Appl. Phys. Lett. **71**, 3239 (1997).
- [57] S.-H. Wei and A. Zunger, Appl. Phys. Lett. **72**, 2011 (1998).

TABLE V: Calculated single particle electron and hole energy level spacings, electron and hole binding energies,  $\Delta E(e, h)$ , electron-electron and electron-hole Coulomb energies, excitonic band gap all in meV, exciton dipole moment and polarization anisotropy for lens shaped and pyramidal  $\text{Ga}_x\text{In}_{1-x}\text{As}$  quantum dots embedded within GaAs.

Geometry % Ga at base,tip,average	Lens Calculations						Pyramid Calc. (g) 200x100Å 0,0,0	Lens Expt. [7, 11]
	(a) 252x35Å 0,0,0	(b) 275x35Å 0,0,0	(c) 252x25Å 0,0,0	(d) 252x35Å 15,15,15	(e) 252x35Å 30,0,15	(f) 275x35Å 15,15,15		
$\delta_{sp} = e_1 - e_0$	65	57	69	58	64	52	108	50
$\delta_{pd} = e_3 - e_2$	68	61	67	60	63	57	64	48
$\delta_{pp} = e_2 - e_1$	2	2	2	2	3	2	26	2
$e_2 - e_1$ (15T)	20	20	18	21	20	17		19
$\delta_{dd} = e_4 - e_3$	4	3	4	4	3	1	23	
$h_0 - h_1$	8	12	16	13	14	11	15	
$h_1 - h_2$	7	6	5	5	6	5	20	
$h_2 - h_3$	6	10	14	13	14	9	1	
$\Delta E(e)$	271	258	251	209	192	204	171	
$\Delta E(h)$	193	186	174	199	203	201	198	
$J_{e_0 e_0}$	31	29	32	29	31	28	40	23
$J_{e_0 e_1}$	25	24	26	24	24	24	35	24
$J_{e_1 e_1}$	25	24	26	25	24	26	36	$\sim 18$
$J_{h_0 h_0}$	30	27	39	32	28	30	31	
$J_{e_0 h_0}$	30	28	35	31	29	29	31	33.3
$K_{h_0 e_0}$	0.15	0.13	0.14	0.15	0.1	0.12	0.2	
$e_0 - h_0 - J_{e_0 h_0}$	1032	1016	1131	1080	1125	1083	1127	1098
$d_{e_0, h_0}$ (Å)	0.16	-0.37	0.5	0.5	1.2	0.5	3.1	
$\lambda = P_{110} : P_{1\bar{1}0}$	1.03	1.01	1.04	1.05	1.08	1.08	1.20	